physica status solidi pss rrl
www.pss-rapid.com

Aerial Photoluminescence Imaging of Photovoltaic Modules

Bernd Doll, Ernst Wittmann, Larry Lüer, Johannes Hepp, Claudia Buerhop-Lutz, Jens A. Hauch, Christoph J. Brabec, and Ian Marius Peters**

On-site imaging of modules in photovoltaic (PV) systems requires contact-free techniques with high throughput and low cost for commercial relevance. Photoluminescence imaging satisfies these requirements, but it has so far not been used for aerial imaging. Such a system faces unique engineering and operating challenges, including the need to mount a light source on the drone and identifying module defects from images taken under low- and nonuniform irradiance. Herein, in-house developed photoluminescence aerial imaging (PLAI) setup is presented and it is demonstrated that it can be used to identify defects even with a difference of excitation intensity of up to 50%. The setup consists of a hexacopter aerial drone equipped with an illumination unit and a near-infrared camera. The unit is capable of partially illuminating full-sized modules at night and capturing the photoluminescence response. In the maiden flight, a throughput of 13.6 PV modules per minute is achieved, and a throughput of 300 PV modules per minute is feasible. It is shown that the setup can be used to detect and identify cracks and potential induced degradation with high levels of confidence. These findings are verified by cross correlation and comparing captured photoluminescence images to electroluminescence images taken indoors.

1. Introduction

Field characterization of photovoltaic (PV) modules enables the detection of defects causing power loss or safety problems at an early stage.[1] Cost-effective on-site examination is essential for commercial relevance and requires high throughput and low invasiveness. Luminescence imaging fulfills these requirements, and it is used in the form of electroluminescence (EL) imaging (ELI) in the field[2,3] and in the lab.[4] ELI gives information about the spatial distribution of the quasi-Fermi-level splitting, allows high image resolution, and enables the detection of numerous types of defects.[5] Yet, ELI is not ideal as it requires accessing the electrical circuitry of the installation to generate a detectable signal.[6] A contact-free alternative is photoluminescence (PL) imaging (PLI), which is well established for inline PV cell[7–9] and indoor PV module inspection.[10] One advantage of PLI at the cell level is that it can be performed prior to the soldering of electrical contacts to the PV cells, eliminating the need for a contacting step on PV modules.[9,10] First outdoor-capable systems are currently developed, either by electrical modulation and sunlight excitation[11] or modulation of selected PV cells can be used for controlling the working point of the inverter or illumination conditions for other PV cells at daytime.[12,13] Both methods need postprocessing to minimize the noise of the sunlight to achieve the PL signal. Another promising technique is the excitation of the PV module per 2D line laser at night-time,[14] but this approach, to our knowledge, has not yet carried out in the field for an entire PV module under real working conditions. A 2D artificial excitation method using broad white light-emitting diodes (LEDs), previously introduced,[15] shows a high reproducibility for defect recognition. A challenge with existing ground-based outdoor PLI systems is the comparably low throughput and the dependence on suitable ground conditions and table spacing in the PV system. To overcome the limitations of ground-based PL imaging setups and to increase throughput further, we have developed a photoluminescence aerial imaging (PLAI) system, capable of performing PLI acquisition at the same pace as the well-established drone-based thermal infrared imaging,[6,16] yet with the benefits of high image resolution and high sensitivity to defects featured by PL.[15]

B. Doll, E. Wittmann, C. Buerhop-Lutz, J. A. Hauch, I. M. Peters
Helmholtz Institute Erlangen-Nürnberg for Renewable Energy
Forschungszentrum Jülich GmbH
Immerwahrstraße 2, 91058 Erlangen, Germany
E-mail: b.doll@fz-juelich.de; i.peters@fz-juelich.de

L. Lüer, C. J. Brabec
Faculty of Engineering
Materials for Electronics and Energy Technology
Friedrich-Alexander University Erlangen-Nürnberg
Martensstraße 7, 91058 Erlangen, Germany

J. Hepp
LayTec AG
Seesener Str. 10 – 13, 10709 Berlin, Germany

The ORCID identification number(s) for the author(s) of this article can be found under https://doi.org/10.1002/pssr.202300059.

DOI: 10.1002/pssr.202300059

physica status solidi pss rrl
www.pss-rapid.com

The main challenge with the drone-mounted system is a partial and nonhomogeneous illumination at low irradiance of the modules, resulting in a superposition of excitation and response. This superposition alters the spatial intensity distribution of light emitted by the solar cells compared to that obtained under laboratory conditions. Altering the light emission pattern is potentially detrimental to the identification of module defects. Here, we test to what degree the intensity distribution measured with our PLAI setup deviates from one obtained using ELI with ideal conditions in the lab using cross-correlation (CC), and we evaluate to what degree this deviation affects our capability to identify module defects. We perform this test on five selected defective PV modules with cracks, shunts, and potential-induced degradation (PID). We find that existing anomalies can be detected with a high level of confidence.

2. PLAI Configuration

In our previous publication,[15] we demonstrated the effectiveness of our large-area PL setup, which utilizes eighteen 100 W broad-white chip-on-board LED modules with a parabolic reflector as optic, similar to the ones we use for the PLAI setup. The custom-built frame of our large-area PL setup provides a high degree of flexibility in terms of the height, tilt, and intensity of both the whole illumination section and each individual LED module. Furthermore, we were able to achieve a standard deviation of approximately 10% in the excitation intensity across the PV module plane for both indoor and outdoor applications. Our results showed that this level of homogeneity is sufficient for reliable defect detection.

Yet also with a standard deviation of excitation intensity of about 50%, defects are detectable. This is demonstrated in **Figure 1** (A-PL) for a PV module in an open circuit condition, where there is no lateral current flow between the PV cells. The standard deviation was calculated from nine irradiance measurements within the whole PV module area. Different PL images under different excitation intensities and excitation intensity distributions are acquired by using a varying amount of LED modules. As the amount of used LED modules homogeneity level and excitation intensity increases from Figure 1 A-PL (two LED modules), B-PL (eight LED modules) to C-PL (18 LED modules), the defect recognition probability increases. However, defects which are verified by the EL image in Figure 1 (D-EL) can be differentiated from PL image features that are caused by nonuniform illumination in Figure 1 (A-PL). The influence of increased nonradiative recombination due to defects (orange square), which depends on the excitation level, is most easily visible at low homogeneity levels, due to the low intensity. In Figure 1 (C-PL), the crack within the orange square is distinctly visible as a crack, rather than solely as a reduction in luminescence intensity at low excitation intensities due to the crack-related open-circuit voltage reduction. Moreover, the cell mismatch indicated by the blue square remains constant for different excitation inhomogeneity distributions. Defects such as PID that affect the parallel resistance can cause similar variations that are difficult to determine, especially at the outer parts of the PV module in images with lower homogeneity level.

From this preliminary experiment we tried to achieve the highest possible homogeneity level for our PLAI setup, but the amount of mountable LED modules is limited to the take-off weight of the whole setup. The aerial setup consists of a custom-made drone frame adjusted by C5UAV GmbH, capable of a take-off weight of 16 kg. It is equipped with four 100 W broad-white LED modules and has a flight time of ≈15 min. However, mounting additional LED modules may significantly reduce the flight time. The filter system consists of a custom-made long-pass filter in front of the camera with a cut-on wavelength of 970 nm and a short-pass filter, namely, "KG5" from Schott. The camera is controlled by an onboard computer and imaging data can be stored on a solid-state drive (SSD). The video signal is transmitted via pixhawk flight control to the remote controller. **Figure 2** depicts the PLAI system standing on a table with the LEDs turned on.

For the experiment presented here, we chose parameters for the indium gallium arsenide (InGaAs) detector camera based on a previously determined trade-off between motion blur and luminescence intensity. In our experiments, we used an "OWL 1280" from Raptor Photonics Limited with a resolution of 1280 × 1024 pixels, set to a 5 ms exposure time, a low aperture of 2.4, and a

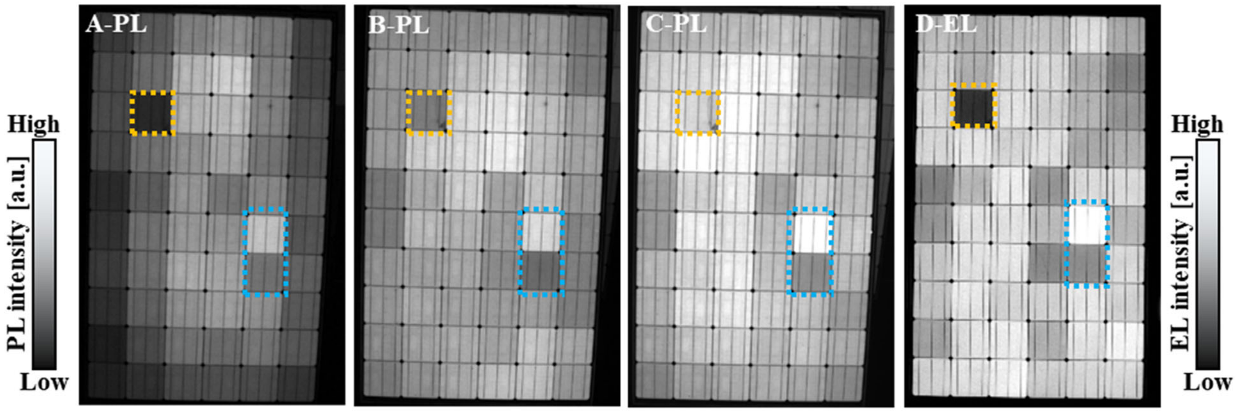

Figure 1. PL images acquired with a variation of the excitation homogeneity and the number of LED modules used. A-PL) 2 LED modules used, B-PL) 8 LED modules used, and C-PL) 18 LED modules used with a mean excitation intensity of 74 W m^{-2} and a standard deviation of ±9.7%. EL image in (D-EL) with an excitation current of 100 mA for comparison. The orange and blue squares highlight abnormalities that are visible in all images, as discussed in the text.

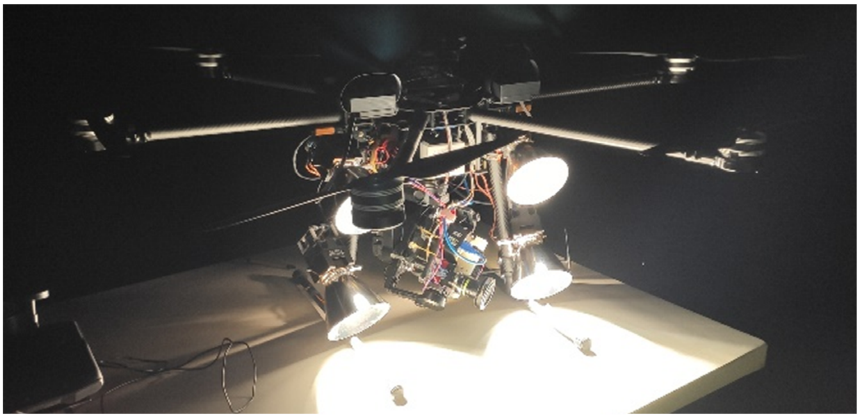

Figure 2. The PLAI setup with four switched-on LED modules and a take-off weight of about 16 kg.

lens focal length of 35 mm for a camera-to-PV-module distance of roughly 5 m.[17] These parameters allow high-quality mobile video recording without motion blur effects at a frame rate of about 10 Hz.

The excitation intensity in the PV module plane was estimated to be around 10–20 W m^{-12}, with a pattern from the highest intensity on the upper part of the PV modules and the lowest intensity at the lower parts of the PV modules, which includes a schematic sketch and an example of PL image, as shown in **Figure 3** as schematic sketch together with a resulting PL image as example. Using a module with low variation between cells, as it is the case for the PV module shown in Figure 3 (except for the three defective cells), allowed us to explore the homogeneity of the excitation for a given illumination. However, the homogeneity level was not perfect, with a variation of about 50% of the excitation intensity over the whole PV module plane, for the PLAI measurements. The reason is that the homogeneity adjustment for just four LED modules is difficult to set and reproduce. Especially, a strong difference between the upper and lower half of the PV modules can be determined. Whether defects are still detectable is discussed in the next section.

During the PL flight, different PV modules with different PV technologies were analyzed. The PV modules and their positioning, together with the corresponding technology and performance parameters, are summarized in **Table 1**.

PV module #1, containing monocrystalline solar cells, has cracks mode A in the upper part, which lead to a reduction in open-circuit voltage (V_{OC}). These cracks decrease the luminescence intensity, especially at low carrier injection, as is the case for the PLAI excitation. PV module #2, with shingled passivated emitter and rear cells (PERC), exhibits strong local scratches in the backsheet of unknown origin, probably due to hard local hits, to damage the rear side of the Si material, resulting in reduced luminescence intensity for three cells. PV module #3, using polycrystalline solar cells, was artificially degraded with an applied potential and shows signs of PID. PV module #4 contains half-cut cells connected without gap ("no gap module"). This module was aged with our mechanical stress setup, resulting in severe cell cracking and cell displacement in its center. PV module #5, a module with mono-c PERCs, has cracks in one cell, potentially caused by transportation.

3. Results

3.1. Analysis of PL Videos

In **Figure 4**, the EL images (labeled #1-EL to #5-EL) and PL images (labeled #1-PL to #5-PL) of the five PV modules described

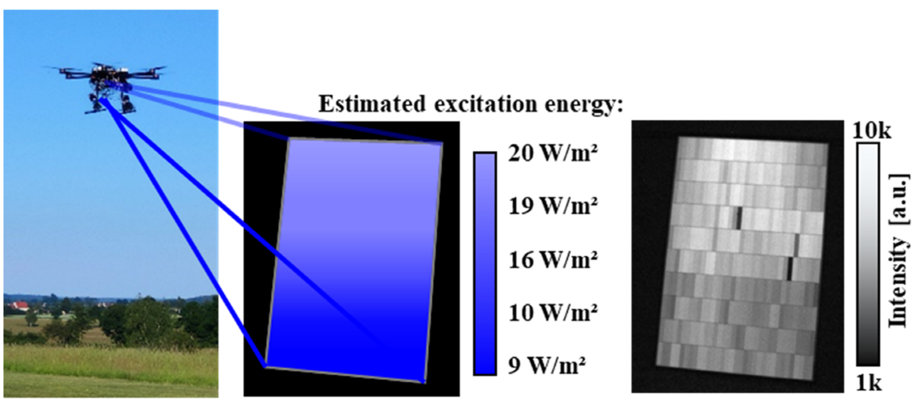

Figure 3. The PLAI setup during test flight at daylight connected to a schematic sketch for the estimated excitation energy and corresponding PL images of PV module #2 as example.

Table 1. Summary of the PV module #1-#5 highlighting their technologies and defects.

PV modulear arrangement	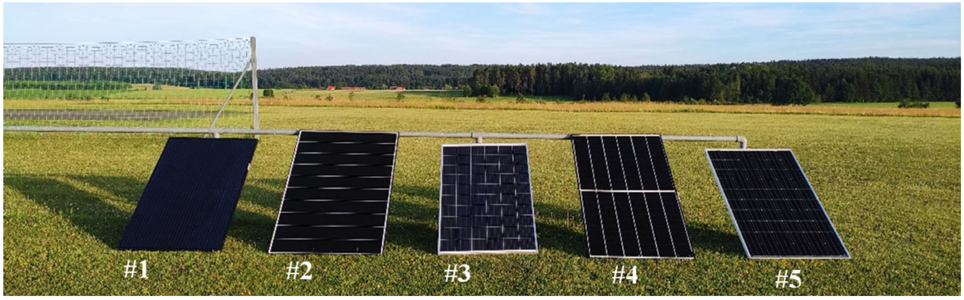				
PV module	#1	#2	#3	#4	#5
PV technology	Monocrystalline	Shingled PERC	Polycrystalline	No-gap half-cut cell	Mono-c PERC
Defect	Cracks	Backside hits to Si	PID	Crack shunted	One cracked cell
Pattern	Reduced PL intensity of the cracked cells	3 cell with low PL intensity	Typical chessboard pattern	Center cells with low PLintensity	One cell with low PL intensity

in Table 1 and labeled #1 to #5 are displayed. The EL images were taken in the lab with a low excitation of 100 mA and an integration time of 30 s using a silicon camera. They offer a clear view of the specific defects of the PV modules and the defect pattern can be easily identified. To compare the detectability of defects with the PLAI setup, the PL images were captured outdoors using the PLAI system and an integration time of 5 ms. The contrast of each PL image was optimized for better appearance.

To quantify the detectability of defects and the level of correlation in both image modalities and to prove that with our PLAI setup the same defects are detectable as for indoor EL images, CC images are calculated. A visualization of the CC results is shown in Figure 4 in the bottom row for all five investigated modules. CC is a method used to identify similarities between two images by comparing the shift of one image relative to the other. The CC coefficient is a measure of the similarity between the two images.

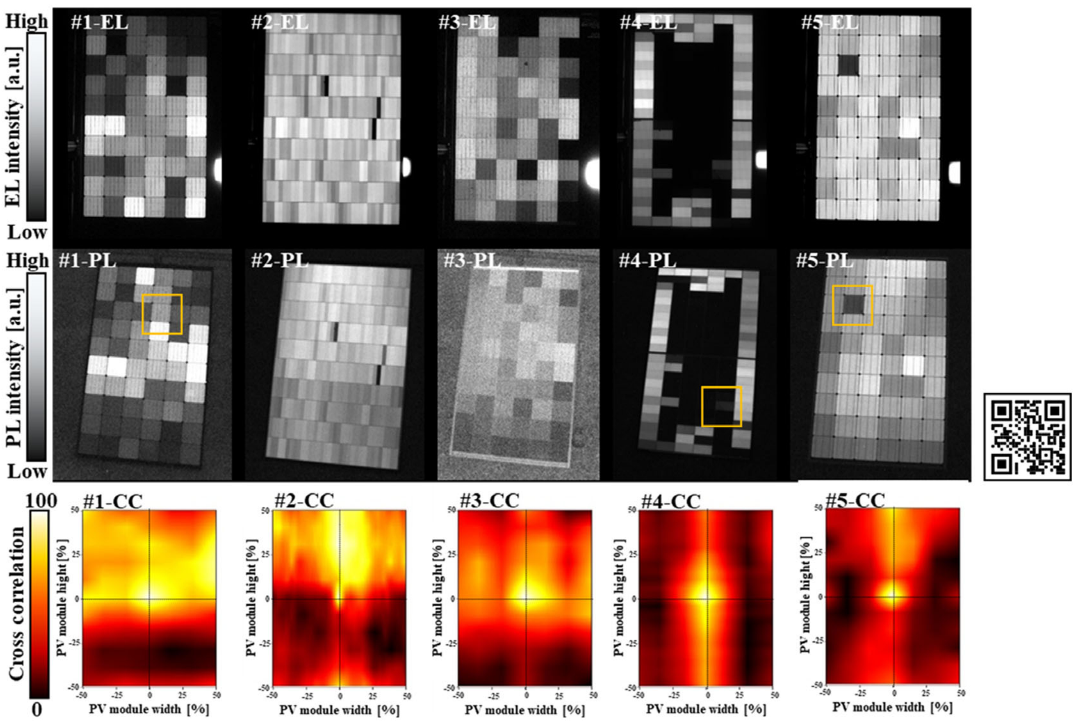

Figure 4. #1-EL to #5-EL images for the PV modules #1-#5 with an excitation of 100 mA and an integration time 30 s taken with a Si camera in the lab as ground truth. In the right lower corner of the EL images, a reference cell is visible which is used for quality control. #1-PL to #5-PL image screenshots of all of the PV modules #1-#5 taken with the PLAI system from the PL video and an integration time of 5 ms. The orange squares indicate the areas used for detailed analysis in Figure 4. The PL video is accessible via QR-code and link https://youtu.be/BayU7MCfsYc. #1-CC to #5-CC shows the normalized 2D CC values of the PL images correlation to the EL images.

The CC image is normalized from 0% with the lowest similarity to 100% with the highest similarity. For the calculation, the CC images with the same amount of pixels are necessary; therefore, for each PV cell and each luminescence modality, mean values are calculated and reconstructed to 6 times 10 pixels for a 60 cell PV module. Summarized, the pixels in CC images are calculated with the reconstructed images of mean EL intensity $\overline{EL}$ and mean PL intensity $\overline{PL}$ values of each PV cell with the coordinates x, y in percentage of the image dimensions, according to ref. [18]

$$CC[x, y] = \frac{1}{x_{max} \cdot y_{max}} \sum_{i,j} \overline{EL}(x+i, y+j) \times \overline{PL}(i,j) \qquad (1)$$

Each CC image shows the strongest correlation for direct overlaying EL and PL image at the center position (0%/0%), indicating a correlation between EL and PL images. For PV modules #1-#3, lower correlations for a negative y-axis shift and high correlations for positive y-axis shift are reached mainly due to excitation inhomogeneity of the PLAI system. For PV module #4, the CC image shows the expected high correlation in y-direction due to the low luminescence intensities in the center of the PV module. With regard to the CC images, we observed the expected diamond-like patterns around the center in all images except for PV module #2. These patterns were formed as expected, given that the PV cells have a rectangular shape. However, PV module #2 has a unique cell geometry compared to the other modules, and as a result, we observed a significantly different pattern in its CC images. This observation is in line with our expectations and highlights the impact of PV cell geometry on the resulting image patterns.

The contrast for the PL video, accessible through the link in the figure caption or the QR-code in the image, was optimized globally to give a qualitative comparison of the PL response of the different PV modules. The PL video can be used to differentiate between the low-homogeneity effects of the excitation resulting in an excitation pattern fixed in the image position and the defect patterns fixed due to different recombination parameters on the PV modules. To clearly identify different defects, machine learning algorithms can be trained to distinguish between these two patterns.

PV modules #2, #4, and #5 have high signal-to-noise ratios (SNR) and defective cells are clearly visible. PV modules #2 and #4 have a SNR of 18 and PV module #5 has a SNR of 9. For PV module #1, the influence of reduced V_{OC} would not be as visible at higher excitation intensities. To demonstrate the visibility of cracks in the PL images captured with the PLAI setup, we performed an analysis of magnified image sections that were marked with orange squares in Figure 4 of the PV modules #1, #4, and #5 as shown in **Figure 5**. In this analysis, we present all magnified PL sections purely and with a determined crack pattern overlaid on top of the images. The crack patterns were determined by various experts who had no prior knowledge of the EL image. Our findings, as depicted in Figure 5, indicate that cracks are indeed detectable in the PLAI images.

The PL image of PV module #3, with a low PL intensity level, is noisy, but the typical PID pattern,[19] with various influence of

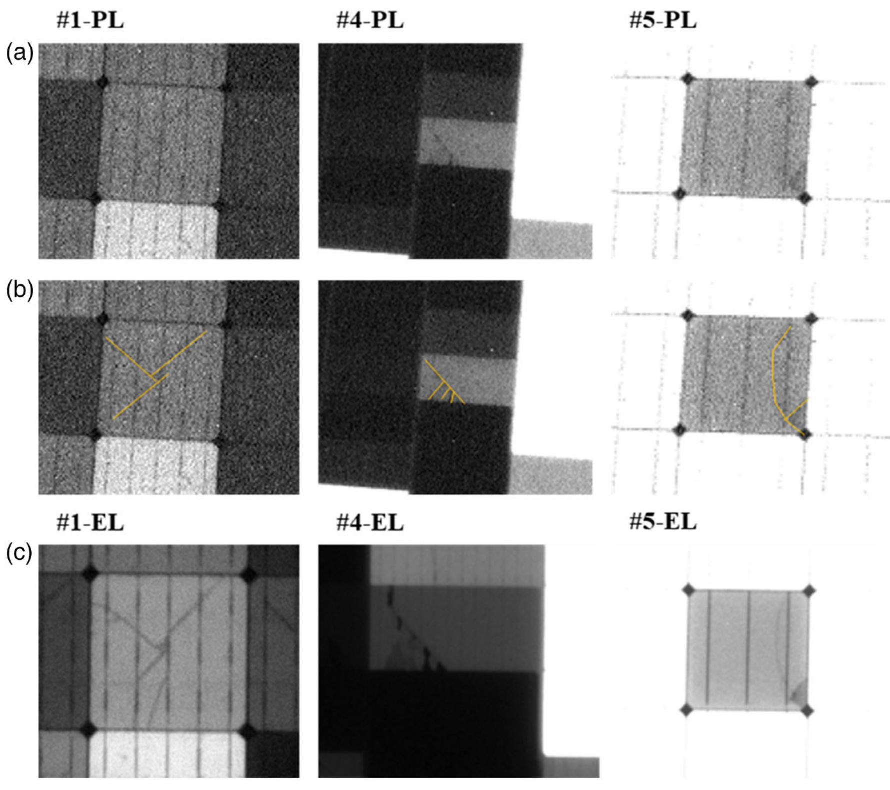

Figure 5. Magnified PL images and manual crack detection. a) Magnified PL images (#1-PL, #4-PL, and #5-PL) marked in Figure 4 are shown purely and b) with a determined crack pattern. c) Corresponding EL images (#1-EL, #4-EL, and #5-EL) from the same PV module position are included as ground truth values for crack detection, which was carried out by PV experts.

the parallel resistance for the different PV cells and therefore various PV cell luminescence intensities, is discernible. During acquisition of the PL video, accessible with the QR-code in Figure 4, roughly a throughput of 13.6 PV modules min^{-1} and a flight speed of about $1.8\,\text{m}\,\text{s}^{-1}$ were reached. The proven throughput of 13.6 PV modules min^{-1} is already the highest one among other contactless luminescence imaging methods that we are aware of. The contactless switching modulation methods shown by the research group from the University of New South Wales[12] has a throughput of about 10 PV modules min^{-1}. Laser-induced luminescence, presented by the research group of the Technical University of Denmark,[20] shows promising results but was not used at commercial PV installations and therefore a throughput could not yet be determined.

For PV module #2, the effect of the inhomogeneous illumination is apparent, resulting in lower brightness of the lower module part. Yet, the three defective cells visible in EL can also be found here. Additionally, the defects and cell intensity distribution are recognizable for the PV modules #4 and #5. PV module #3 has the lowest PL signal, as expected from its age and polycrystallinity shown by Green et al.[21] for different PV cell technologies. The defect recognition due to the low PL signal level is affected by the noise of the InGaAs camera with a standard deviation within the same level as the PL signal level.

In all images, the specific patterns indicative of each defect are present in the EL reference images as well as in the ones captured with PLAI. Consequently, we expect a mathematically expressible correlation between the images. Yet, the PL images also exhibit alterations of the pattern due to excitation inhomogeneity during the measurements. These inhomogeneities may constitute a complication for automated pattern recognition and defect detection.

4. Conclusion

In this study, we propose a novel, noninvasive method for detecting defects in PV modules using PLAI. We utilized a drone-mounted system to perform PLI acquisition, enabling high-throughput detection at the same pace as well-established drone-based thermal infrared imaging. However, one major challenge of our system is the partial and nonhomogeneous illumination at low irradiance, which can alter the spatial intensity distribution of light emitted by the PV cells and potentially hinder the identification of PV module defects. To overcome this challenge, we compared the intensity distribution of PL images taken with the PLAI setup to that of EL images taken under ideal laboratory conditions using CC. We found that despite the nonhomogeneous excitation intensity, our PLAI setup can detect the same defect patterns as indoor EL images, including various types of defects such as cracks, PID, and scratches in the backsheet.

Although our PLAI setup is limited due to its take-off weight and the use of only four LED lamps for PL excitation, we demonstrated that many defects can be detected with high correlation using our system. However, defects resulting in low efficiency and overall low light emission of a module, such as those exhibited by module #3, result in high levels of noise and may require higher excitation intensities for reliable imaging of defects. Despite this limitation, our PLAI setup offers several advantages, including no contact with PV modules and the ability to conduct inspections from the air, potentially enabling high-throughput inspections of large-scale installations.

In our presented experiment, we achieved a rate of 13.6 PV modules measured per minute, with the potential to increase this to up to 300 PV modules per minute by increasing flight speed and image acquisition. Our future work will focus on demonstrating the cost-effectiveness and reliability of PLAI for detecting defects in photovoltaic systems in the PV industry.

Overall, we believe that our proposed PLAI method has the potential to become a valuable tool for the PV industry, offering a high-throughput and noninvasive approach to detecting defects in PV modules. By overcoming the challenge of partial and nonhomogeneous illumination, we have demonstrated that our system can reliably detect various types of defects, even with low excitation intensities. As we continue to improve and optimize our PLAI setup, we aim to provide a cost-effective and efficient solution for widespread use in the PV industry.

Acknowledgements

The authors gratefully acknowledge the State of Bavaria for financial funding of the project PV-Tera (No. 446521a/20/5) and the German Federal Ministry for Economics and Climate Action (BMWK) for financial funding of the project iPV4.0 (FKZ: 0324286D), COSIMA (FKZ: 032429A) and dig4morE (FKZ: 03EE1090B). The authors sincerely thank the SUNSET Energietechnik GmbH for supporting the project with PV modules. This article benefited from the use of ChatGPT to improve its English wording and grammar.

Open Access funding enabled and organized by Projekt DEAL.

Conflict of Interest

The authors declare no conflict of interest.

Data Availability Statement

The data that support the findings of this study are available on request from the corresponding author. The data are not publicly available due to privacy or ethical restrictions.

Keywords

aerial inspection, photoluminescence, photovoltaic

Received: February 13, 2023
Revised: April 18, 2023
Published online: May 9, 2023

[1] K. Berger, B. Kubicek, G. Eder, Y. Voronko, M. Weiss, G. Oreski, M. Knausz, T. Koch, J. Wassermann, *28 Symposium Photovoltaische Solarenergie*, Austria, **2013**, https://publications.ait.ac.at/de/publications/innovative-nichtzerst%C3%B6rende-methoden-zur-untersuchung-von-photovo-10.

[2] U. Jahn, M. Herz, M. Köntges, D. Parlevliet, M. Paggi, I. Tsanakas, J. S. Stein, K. A. Berger, S. Ranta, R. H. French, M. Richter, T. Tanahashi, *Report IEA-PVPS T13-10:2018*, Rheine, Germany **2018**, https://iea-pvps.org/key-topics/review-on-ir-and-el-imaging-for-pv-field-applications/.

[3] S. Koch, T. Weber, C. Sobottka, A. Fladung, P. Clemens, in *32nd European Photovoltaic Solar Energy Conf. and Exhibition*, WIP Wirtschaft und Infrastruktur GmbH & Co Planungs KG, München, Germany **2016**, pp. 1736–1740.
[4] K. G. Bedrich, J. Chai, Y. Wang, A. G. Aberle, M. Bliss, M. Bokalic, B. Doll, M. Köntges, A. Huss, J. Lopez-Garcia, Y. S. Khoo, *35th Eur. Photovolt. Sol. Energy Conf. Exhib.*, WIP Wirtschaft und Infrastruktur GmbH & Co Planungs KG, München, Germany **2018**, pp. 1049–1056.
[5] T. Fuyuki, H. Kondo, T. Yamazaki, Y. Takahashi, Y. Uraoka, *Appl. Phys. Lett.* **2005**, *86*, 1.
[6] J. A. Tsanakas, L. Ha, C. Buerhop, *Renew. Sustain. Energy Rev.* **2016**, *62*, 695.
[7] M. Kasemann, L. M. Reindl, B. Michl, W. Warta, A. Schütt, J. Carstensen, *IEEE J. Photovoltaics* **2012**, *2*, 181.
[8] T. Trupke, R. A. Bardos, in *Conf. Record of the Thirty-first IEEE Photovoltaic Specialists Conf.*, Lake Buena Vista, FL **2005**, pp. 903–906, https://doi.org/10.1109/PVSC.2005.1488277.
[9] T. Trupke, R. A. Bardos, M. C. Schubert, W. Warta, *Appl. Phys. Lett.* **2006**, *89*, 1.
[10] I. Zafirovska, M. K. Juhl, T. Trupke, in *2018 IEEE 7th World Conf. on Photovoltaic Energy Conversion (WCPEC) (A Joint Conf. of 45th IEEE PVSC, 28th PVSEC & 34th EU PVSEC)*, Waikoloa, HI **2018**, pp. 1364–1369, https://doi.org/10.1109/PVSC.2018.8547434.
[11] L. Stoicescu, M. Reuter, J. H. Werner, in *29th European Photovoltaics Solar Energy Conf. and Exhibition*, WIP Wirtschaft und Infrastruktur GmbH & Co Planungs KG, München, Germany **2014**, pp. 2553–2554.
[12] O. Kunz, G. Rey, M. K. Juhl, T. Trupke, in *IEEE 48th Photovoltaic Specialists Conf. (PVSC)*, Fort Lauderdale, FL **2021**, pp. 0346–0350, https://doi.org/10.1109/PVSC43889.2021.9519109.
[13] R. Bhoopathy, O. Kunz, M. Juhl, T. Trupke, Z. Hameiri, *Prog. Photovoltaics Res. Appl.* **2017**, *26*, 69.
[14] G. A. dos Reis Benatto, C. Mantel, N. Riedel, A. A. Santamaria Lancia, S. Thorsteinsson, P. B. Poulsen, S. Forchhammer, A. Thorseth, C. Dam-Hansen, K. H. B. Frederiksen, J. Vedde, M. Larsen, H. Voss, H. Parikh, S. Spataru, D. Sera, in *IEEE 7th World Conf. on Photovoltaic Energy Conversion (WCPEC) (A Joint Conf. of 45th IEEE PVSC, 28th PVSEC & 34th EU PVSEC)*, Waikoloa, HI **2018**, pp. 0400–0404, https://doi.org/10.1109/PVSC.2018.8547628.
[15] B. Doll, J. Hepp, M. Hoffmann, R. Schuler, C. Buerhop-Lutz, I. M. Peters, J. A. Hauch, A. Maier, C. J. Brabec, *IEEE J. Photovoltaics* **2021**, *11*, 1419.
[16] C. Buerhop, T. Pickel, H. Scheuerpflug, C. Camus, J. Hauch, C. J. Brabec, in *Proc. SPIE 9938, Reliability of Photovoltaic Cells, Modules, Components, and Systems IX*, **2016**, p. 99380L, https://doi.org/10.1117/12.2237821 (accessed: September 2016).
[17] B. Doll, T. Pickel, O. Schreer, C. Zetzmann, J. Hepp, J. Teubner, C. Buerhop, J. A. Hauch, C. Camus, C. J. Brabec, *Opt. Eng.* **2019**, *58*, 1.
[18] K. D. Tönnies, G. der Bildverarbeitung. Pearson Studium, **2005**, ISBN: 3827371554.
[19] M. Köntges, S. Kurtz, C. E. Packard, U. Jahn, K. Berger, K. Kato, T. Friesen, H. Liu, M. Van Iseghem, *Report IEA-PVPS T13-01:2014*, Rheine, Germany **2014**, https://iea-pvps.org/key-topics/review-of-failures-of-photovoltaic-modules-final/.
[20] G. A. Dos Reis Benatto, M. Chi, O. B. Jensen, A. A. S. Lancia, N. Riedel, B. Iandolo, R. S. Davidsen, O. Hansen, S. Thorsteinsson, P. B. Poulsen, in *IEEE 7th World Conf. on Photovoltaic Energy Conversion (WCPEC) (A Joint Conf. of 45th IEEE PVSC, 28th PVSEC & 34th EU PVSEC)*, **2018**, pp. 0395–0399.
[21] M. A. Green, J. Zhao, A. Wang, P. J. Reece, M. Gal, *Nature* **2001**, *412*, 805.